

Ratio of Isolated Photon Cross Sections in $p\bar{p}$ Collisions at $\sqrt{s} = 630$ and 1800 GeV

V. M. Abazov,²³ B. Abbott,⁵⁷ A. Abdesselam,¹¹ M. Abolins,⁵⁰ V. Abramov,²⁶ B. S. Acharya,¹⁷ D. L. Adams,⁵⁹ M. Adams,³⁷ S. N. Ahmed,²¹ G. D. Alexeev,²³ A. Alton,⁴⁹ G. A. Alves,² N. Amos,⁴⁹ E. W. Anderson,⁴² Y. Arnaud,⁹ C. Avila,⁵ M. M. Baarmand,⁵⁴ V. V. Babintsev,²⁶ L. Babukhadia,⁵⁴ T. C. Bacon,²⁸ A. Baden,⁴⁶ B. Baldin,³⁶ P. W. Balm,²⁰ S. Banerjee,¹⁷ E. Barberis,³⁰ P. Baringer,⁴³ J. Barreto,² J. F. Bartlett,³⁶ U. Bassler,¹² D. Bauer,²⁸ A. Bean,⁴³ F. Beaudette,¹¹ M. Begel,⁵³ A. Belyaev,³⁵ S. B. Beri,¹⁵ G. Bernardi,¹² I. Bertram,²⁷ A. Besson,⁹ R. Beuselinck,²⁸ V. A. Bezzubov,²⁶ P. C. Bhat,³⁶ V. Bhatnagar,¹¹ M. Bhattacharjee,⁵⁴ G. Blazey,³⁸ F. Blekman,²⁰ S. Blessing,³⁵ A. Boehnlein,³⁶ N. I. Bojko,²⁶ F. Borchering,³⁶ K. Bos,²⁰ T. Bose,⁵² A. Brandt,⁵⁹ R. Breedon,³¹ G. Briskin,⁵⁸ R. Brock,⁵⁰ G. Brooijmans,³⁶ A. Bross,³⁶ D. Buchholz,³⁹ M. Buehler,³⁷ V. Buescher,¹⁴ V. S. Burtovoi,²⁶ J. M. Butler,⁴⁷ F. Canelli,⁵³ W. Carvalho,³ D. Casey,⁵⁰ Z. Casilum,⁵⁴ H. Castilla-Valdez,¹⁹ D. Chakraborty,³⁸ K. M. Chan,⁵³ S. V. Chekulaev,²⁶ D. K. Cho,⁵³ S. Choi,³⁴ S. Chopra,⁵⁵ J. H. Christenson,³⁶ M. Chung,³⁷ D. Claes,⁵¹ A. R. Clark,³⁰ J. Cochran,³⁴ L. Coney,⁴¹ B. Connolly,³⁵ W. E. Cooper,³⁶ D. Coppage,⁴³ S. Crépe-Renaudin,⁹ M. A. C. Cummings,³⁸ D. Cutts,⁵⁸ G. A. Davis,⁵³ K. Davis,²⁹ K. De,⁵⁹ S. J. de Jong,²¹ K. Del Signore,⁴⁹ M. Demarteau,³⁶ R. Demina,⁴⁴ P. Demine,⁹ D. Denisov,³⁶ S. P. Denisov,²⁶ S. Desai,⁵⁴ H. T. Diehl,³⁶ M. Diesburg,³⁶ S. Doulas,⁴⁸ Y. Ducros,¹³ L. V. Dudko,²⁵ S. Duensing,²¹ L. Duflot,¹¹ S. R. Dugad,¹⁷ A. Duperrin,¹⁰ A. Dyshkant,³⁸ D. Edmunds,⁵⁰ J. Ellison,³⁴ V. D. Elvira,³⁶ R. Engelmann,⁵⁴ S. Eno,⁴⁶ G. Eppley,⁶¹ P. Ermolov,²⁵ O. V. Eroshin,²⁶ J. Estrada,⁵³ H. Evans,⁵² V. N. Evdokimov,²⁶ T. Fahland,³³ S. Feher,³⁶ D. Fein,²⁹ T. Ferbel,⁵³ F. Filthaut,²¹ H. E. Fisk,³⁶ Y. Fisyak,⁵⁵ E. Flattum,³⁶ F. Fleuret,¹² M. Fortner,³⁸ H. Fox,³⁹ K. C. Frame,⁵⁰ S. Fu,⁵² S. Fuess,³⁶ E. Gallas,³⁶ A. N. Galyaev,²⁶ M. Gao,⁵² V. Gavrilov,²⁴ R. J. Genik II,²⁷ K. Genser,³⁶ C. E. Gerber,³⁷ Y. Gershtein,⁵⁸ R. Gilmartin,³⁵ G. Ginter,⁵³ B. Gómez,⁵ G. Gómez,⁴⁶ P. I. Goncharov,²⁶ J. L. González Solís,¹⁹ H. Gordon,⁵⁵ L. T. Goss,⁶⁰ K. Gounder,³⁶ A. Goussiou,²⁸ N. Graf,⁵⁵ G. Graham,⁴⁶ P. D. Grannis,⁵⁴ J. A. Green,⁴² H. Greenlee,³⁶ Z. D. Greenwood,⁴⁵ S. Grinstein,¹ L. Groer,⁵² S. Grünendahl,³⁶ A. Gupta,¹⁷ S. N. Gurzhiev,²⁶ G. Gutierrez,³⁶ P. Gutierrez,⁵⁷ N. J. Hadley,⁴⁶ H. Haggerty,³⁶ S. Hagopian,³⁵ V. Hagopian,³⁵ R. E. Hall,³² P. Hanlet,⁴⁸ S. Hansen,³⁶ J. M. Hauptman,⁴² C. Hays,⁵² C. Hebert,⁴³ D. Hedin,³⁸ J. M. Heinmiller,³⁷ A. P. Heinson,³⁴ U. Heintz,⁴⁷ T. Heuring,³⁵ M. D. Hildreth,⁴¹ R. Hirosky,⁶² J. D. Hobbs,⁵⁴ B. Hoeneisen,⁸ Y. Huang,⁴⁹ R. Illingworth,²⁸ A. S. Ito,³⁶ M. Jaffré,¹¹ S. Jain,¹⁷ R. Jesik,²⁸ K. Johns,²⁹ M. Johnson,³⁶ A. Jonckheere,³⁶ H. Jöstlein,³⁶ A. Juste,³⁶ W. Kahl,⁴⁴ S. Kahn,⁵⁵ E. Kajfasz,¹⁰ A. M. Kalinin,²³ D. Karmanov,²⁵ D. Karmgard,⁴¹ R. Kehoe,⁵⁰ A. Khanov,⁴⁴ A. Kharchilava,⁴¹ S. K. Kim,¹⁸ B. Klima,³⁶ B. Knuteson,³⁰ W. Ko,³¹ J. M. Kohli,¹⁵ A. V. Kostritskiy,²⁶ J. Kotcher,⁵⁵ B. Kothari,⁵² A. V. Kotwal,⁵² A. V. Kozelov,²⁶ E. A. Kozlovsky,²⁶ J. Krane,⁴² M. R. Krishnaswamy,¹⁷ P. Krivkova,⁶ S. Krzywdzinski,³⁶ M. Kubantsev,⁴⁴ S. Kuleshov,²⁴ Y. Kulik,⁵⁴ S. Kunori,⁴⁶ A. Kupco,⁷ V. E. Kuznetsov,³⁴ G. Landsberg,⁵⁸ W. M. Lee,³⁵ A. Leflat,²⁵ C. Leggett,³⁰ F. Lehner,^{36,*} J. Li,⁵⁹ Q. Z. Li,³⁶ X. Li,⁴ J. G. R. Lima,³ D. Lincoln,³⁶ S. L. Linn,³⁵ J. Linnemann,⁵⁰ R. Lipton,³⁶ A. Lucotte,⁹ L. Lueking,³⁶ C. Lundstedt,⁵¹ C. Luo,⁴⁰ A. K. A. Maciel,³⁸ R. J. Madaras,³⁰ V. L. Malyshev,²³ V. Manankov,²⁵ H. S. Mao,⁴ T. Marshall,⁴⁰ M. I. Martin,³⁸ K. M. Mauritz,⁴² B. May,³⁹ A. A. Mayorov,⁴⁰ R. McCarthy,⁵⁴ T. McMahon,⁵⁶ H. L. Melanson,³⁶ M. Merkin,²⁵ K. W. Merritt,³⁶ C. Miao,⁵⁸ H. Miettinen,⁶¹ D. Mihalcea,³⁸ C. S. Mishra,³⁶ N. Mokhov,³⁶ N. K. Mondal,¹⁷ H. E. Montgomery,³⁶ R. W. Moore,⁵⁰ M. Mostafa,¹ H. da Motta,² E. Nagy,¹⁰ F. Nang,²⁹ M. Narain,⁴⁷ V. S. Narasimham,¹⁷ N. A. Naumann,²¹ H. A. Neal,⁴⁹ J. P. Negret,⁵ S. Negroni,¹⁰ T. Nunnemann,³⁶ D. O'Neil,⁵⁰ V. Oguri,³ B. Olivier,¹² N. Oshima,³⁶ P. Padley,⁶¹ L. J. Pan,³⁹ K. Papageorgiou,³⁷ A. Para,³⁶ N. Parashar,⁴⁸ R. Partridge,⁵⁸ N. Parua,⁵⁴ M. Paterno,⁵³ A. Patwa,⁵⁴ B. Pawlik,²² J. Perkins,⁵⁹ O. Peters,²⁰ P. Pétroff,¹¹ R. Piegai,¹ B. G. Pope,⁵⁰ E. Popkov,⁴⁷ H. B. Prosper,³⁵ S. Protopopescu,⁵⁵ M. B. Przybycien,³⁹ J. Qian,⁴⁹ R. Raja,³⁶ S. Rajagopalan,⁵⁵ E. Ramberg,³⁶ P. A. Rapidis,³⁶ N. W. Reay,⁴⁴ S. Reucroft,⁴⁸ M. Ridel,¹¹ M. Rijssenbeek,⁵⁴ F. Rizatdinova,⁴⁴ T. Rockwell,⁵⁰ M. Roco,³⁶ C. Royon,¹³ P. Rubinov,³⁶ R. Ruchti,⁴¹ J. Rutherford,²⁹ B. M. Sapiro,²³ G. Sajot,⁹ A. Santoro,² L. Sawyer,⁴⁵ R. D. Schamberger,⁵⁴ H. Schellman,³⁹ A. Schwartzman,¹ N. Sen,⁶¹ E. Shabalina,³⁷ R. K. Shivpuri,¹⁶ D. Shpakov,⁴⁸ M. Shupe,²⁹ R. A. Sidwell,⁴⁴ V. Simak,⁷ H. Singh,³⁴ J. B. Singh,¹⁵ V. Sirotenko,³⁶ P. Slattery,⁵³ E. Smith,⁵⁷ R. P. Smith,³⁶ R. Snihur,³⁹ G. R. Snow,⁵¹ J. Snow,⁵⁶ S. Snyder,⁵⁵ J. Solomon,³⁷ Y. Song,⁵⁹ V. Sorín,¹ M. Sosebee,⁵⁹ N. Sotnikova,²⁵ K. Soustruznik,⁶ M. Souza,² N. R. Stanton,⁴⁴ G. Steinbrück,⁵² R. W. Stephens,⁵⁹ F. Stichelbaut,⁵⁵ D. Stoker,³³ V. Stolin,²⁴ A. Stone,⁴⁵ D. A. Stoyanova,²⁶ M. A. Strang,⁵⁹ M. Strauss,⁵⁷ M. Strovink,³⁰ L. Stutte,³⁶ A. Sznajder,³ M. Talby,¹⁰ W. Taylor,⁵⁴ S. Tentindo-Repond,³⁵ S. M. Tripathi,³¹ T. G. Trippe,³⁰

A. S. Turcot,⁵⁵ P. M. Tuts,⁵² V. Vaniev,²⁶ R. Van Kooten,⁴⁰ N. Varelas,³⁷ L. S. Vertogradov,²³ F. Villeneuve-Seguiet,¹⁰
 A. A. Volkov,²⁶ A. P. Vorobiev,²⁶ H. D. Wahl,³⁵ H. Wang,³⁹ Z.-M. Wang,⁵⁴ J. Warchol,⁴¹ G. Watts,⁶³ M. Wayne,⁴¹
 H. Weerts,⁵⁰ A. White,⁵⁹ J. T. White,⁶⁰ D. Whiteson,³⁰ J. A. Wightman,⁴² D. A. Wijngaarden,²¹ S. Willis,³⁸
 S. J. Wimpenny,³⁴ J. Womersley,³⁶ D. R. Wood,⁴⁸ Q. Xu,⁴⁹ R. Yamada,³⁶ P. Yamin,⁵⁵ T. Yasuda,³⁶ Y. A. Yatsunenko,²³
 K. Yip,⁵⁵ S. Youssef,³⁵ J. Yu,³⁶ Z. Yu,³⁹ M. Zanabria,⁵ X. Zhang,⁵⁷ H. Zheng,⁴¹ B. Zhou,⁴⁹ Z. Zhou,⁴² M. Zielinski,⁵³
 D. Zieminska,⁴⁰ A. Zieminski,⁴⁰ V. Zutshi,⁵⁵ E. G. Zverev,²⁵ and A. Zylberstejn¹³

(D0 Collaboration)

- ¹Universidad de Buenos Aires, Buenos Aires, Argentina
²LAFEX, Centro Brasileiro de Pesquisas Físicas, Rio de Janeiro, Brazil
³Universidade do Estado do Rio de Janeiro, Rio de Janeiro, Brazil
⁴Institute of High Energy Physics, Beijing, People's Republic of China
⁵Universidad de los Andes, Bogotá, Colombia
⁶Charles University, Center for Particle Physics, Prague, Czech Republic
⁷Institute of Physics, Academy of Sciences, Center for Particle Physics, Prague, Czech Republic
⁸Universidad San Francisco de Quito, Quito, Ecuador
⁹Institut des Sciences Nucléaires, IN2P3-CNRS, Université de Grenoble I, Grenoble, France
¹⁰CPPM, IN2P3-CNRS, Université de la Méditerranée, Marseille, France
¹¹Laboratoire de l'Accélérateur Linéaire, IN2P3-CNRS, Orsay, France
¹²LPNHE, Universités Paris VI and VII, IN2P3-CNRS, Paris, France
¹³DAPNIA/Service de Physique des Particules, CEA, Saclay, France
¹⁴Universität Mainz, Institut für Physik, Mainz, Germany
¹⁵Panjab University, Chandigarh, India
¹⁶Delhi University, Delhi, India
¹⁷Tata Institute of Fundamental Research, Mumbai, India
¹⁸Seoul National University, Seoul, Korea
¹⁹CINVESTAV, Mexico City, Mexico
²⁰FOM-Institute NIKHEF and University of Amsterdam/NIKHEF, Amsterdam, The Netherlands
²¹University of Nijmegen/NIKHEF, Nijmegen, The Netherlands
²²Institute of Nuclear Physics, Kraków, Poland
²³Joint Institute for Nuclear Research, Dubna, Russia
²⁴Institute for Theoretical and Experimental Physics, Moscow, Russia
²⁵Moscow State University, Moscow, Russia
²⁶Institute for High Energy Physics, Protvino, Russia
²⁷Lancaster University, Lancaster, United Kingdom
²⁸Imperial College, London, United Kingdom
²⁹University of Arizona, Tucson, Arizona 85721
³⁰Lawrence Berkeley National Laboratory and University of California, Berkeley, California 94720
³¹University of California, Davis, California 95616
³²California State University, Fresno, California 93740
³³University of California, Irvine, California 92697
³⁴University of California, Riverside, California 92521
³⁵Florida State University, Tallahassee, Florida 32306
³⁶Fermi National Accelerator Laboratory, Batavia, Illinois 60510
³⁷University of Illinois at Chicago, Chicago, Illinois 60607
³⁸Northern Illinois University, DeKalb, Illinois 60115
³⁹Northwestern University, Evanston, Illinois 60208
⁴⁰Indiana University, Bloomington, Indiana 47405
⁴¹University of Notre Dame, Notre Dame, Indiana 46556
⁴²Iowa State University, Ames, Iowa 50011
⁴³University of Kansas, Lawrence, Kansas 66045
⁴⁴Kansas State University, Manhattan, Kansas 66506
⁴⁵Louisiana Tech University, Ruston, Louisiana 71272
⁴⁶University of Maryland, College Park, Maryland 20742
⁴⁷Boston University, Boston, Massachusetts 02215
⁴⁸Northeastern University, Boston, Massachusetts 02115
⁴⁹University of Michigan, Ann Arbor, Michigan 48109
⁵⁰Michigan State University, East Lansing, Michigan 48824
⁵¹University of Nebraska, Lincoln, Nebraska 68588
⁵²Columbia University, New York, New York 10027
⁵³University of Rochester, Rochester, New York 14627

⁵⁴State University of New York, Stony Brook, New York 11794

⁵⁵Brookhaven National Laboratory, Upton, New York 11973

⁵⁶Langston University, Langston, Oklahoma 73050

⁵⁷University of Oklahoma, Norman, Oklahoma 73019

⁵⁸Brown University, Providence, Rhode Island 02912

⁵⁹University of Texas, Arlington, Texas 76019

⁶⁰Texas A&M University, College Station, Texas 77843

⁶¹Rice University, Houston, Texas 77005

⁶²University of Virginia, Charlottesville, Virginia 22901

⁶³University of Washington, Seattle, Washington 98195

(Received 13 August 2001; published 30 November 2001)

The inclusive cross section for production of isolated photons has been measured in $p\bar{p}$ collisions at $\sqrt{s} = 630$ GeV with the D0 detector at the Fermilab Tevatron Collider. The photons span a transverse energy (E_T) range from 7–49 GeV and have pseudorapidity $|\eta| < 2.5$. This measurement is combined with the previous D0 result at $\sqrt{s} = 1800$ GeV to form a ratio of the cross sections. Comparison of next-to-leading-order QCD with the measured cross section at 630 GeV and the ratio of cross sections show satisfactory agreement in most of the E_T range.

DOI: 10.1103/PhysRevLett.87.251805

PACS numbers: 13.85.Qk, 12.38.Qk

Within the framework of quantum chromodynamics (QCD), isolated single photons are direct photons: produced from the primary parton-parton interactions. Because the dominant production mechanism for photons of modest transverse energy (E_T) at the Fermilab Tevatron is gluon Compton scattering ($qg \rightarrow \gamma q$), the cross section for direct-photon production is sensitive to the gluon distribution in the proton [1]. A measurement of the final state photons provides a probe of QCD without additional complications from fragmentation and jet identification, providing a powerful and effective means for studying the constituents of hadronic matter.

Previous experiments, at center-of-mass energies of both 630 GeV [2] and 1800 GeV [3,4], have reported photon production in excess of next-to-leading-order (NLO) QCD predictions at low transverse energies ($E_T^{\gamma} \lesssim 30$ GeV). This disagreement with data could result from gluon radiation not included in NLO calculations [5] or because the parton distributions are not well known [6].

In this Letter, we present a measurement of the isolated photon cross section in $p\bar{p}$ collisions for photons in two pseudorapidity regions, $|\eta| < 0.9$ and $1.6 < |\eta| < 2.5$, where $\eta = -\ln \tan \frac{\theta}{2}$ and θ is the polar angle with respect to the proton beam. We compare the production cross section at $\sqrt{s} = 630$ GeV with the previously published D0 results at $\sqrt{s} = 1800$ GeV [3]. A ratio of the cross sections at different energies reduces systematic uncertainties and minimizes the sensitivity to the choice of parton distribution functions (PDF) because the measurements at both energies use the same detector and the same analysis method.

The cross section measurement at 630 GeV uses a sample of 520 nb^{-1} of data recorded in 1995 [7] with the D0 detector at the Fermilab Tevatron [8]. The analysis uses the uranium/liquid argon calorimeter to identify electromagnetic (EM) showers, and the drift chambers in front of the calorimeter to differentiate photon showers from electron showers. The EM calorimeter provides full

azimuthal (ϕ) coverage, and consists of a central cryostat (CC) with $|\eta| \lesssim 1.1$, and two forward cryostats (EC) with $1.4 \lesssim |\eta| \lesssim 4.0$. The EM calorimeter is divided into four longitudinal layers, EM1–EM4, of approximately 2, 2, 7, and 10 radiation lengths, respectively. The EM energy resolution in the central and forward calorimeters is given by $\sigma_E/E = \{15\%/\sqrt{E(\text{GeV})}\} \oplus 0.3\%$.

Photons interacting in the calorimeter are detected using a three-level triggering system. The first level consists of scintillation counters near the beam pipe, which detect inelastic $p\bar{p}$ collisions. The second level requires a minimum energy deposition in a $\Delta\phi \times \Delta\eta = 0.2 \times 0.2$ trigger tower, with thresholds of 2.0, 3.0, and 7.0 GeV. In the final step, calorimeter clusters are formed with corresponding thresholds of 4.5, 8.0, and 14.0 GeV. The trigger efficiency is determined for the 14.0 and 8.0 GeV thresholds by taking the ratio of events passing each trigger criterion to those passing the 8.0 and 4.5 GeV criteria, respectively, in an energy regime where the lower threshold trigger is 100% efficient. Monte Carlo studies of the trigger algorithms show agreement with the data for the two higher energy triggers, and are used to determine the trigger efficiency for the 4.5 GeV trigger. Trigger efficiencies are typically about 20% at the nominal energy threshold and rise to almost 100% a few GeV above the threshold value. Consequently, photon candidates are accepted only for transverse energies of at least 7.35, 10, and 16 GeV for the three triggers, respectively.

Photon candidates are identified as energy clusters located well within the pseudorapidity boundaries of the central calorimeter or the forward calorimeter, and, in the central calorimeter, are located at least 1.6 cm from the azimuthal section boundaries. The event vertex position is required to be within 50 cm of the center of the detector. The resulting geometric acceptance is $A = 0.622 \pm 0.007$ (0.787 ± 0.007) in the central (forward) region. Candidates must pass a series of selection criteria [3] that identify the energy cluster as

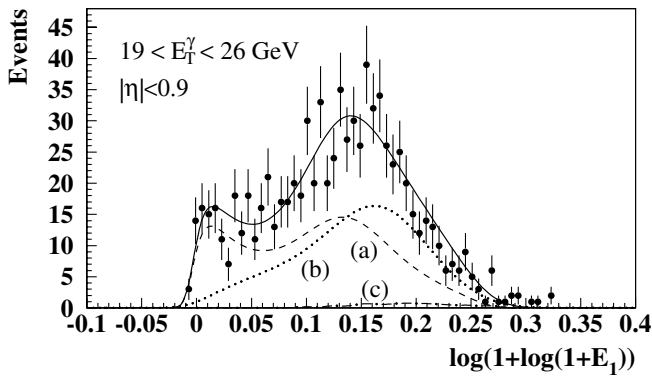


FIG. 1. Distribution of the discriminant, f , for determining photon purity, where E_1 is in units of GeV. Points with error bars indicate data. The dashed, dotted, and dot-dashed lines indicate simulated distributions of (a) single photons, and jet background (b) without and (c) with charged tracks. The solid line depicts a fit sum of all three distributions.

an electromagnetic shower. The total transverse energy near any candidate cluster must satisfy an isolation requirement $E_T^{\mathcal{R} \leq 0.4} - E_T^{\mathcal{R} \leq 0.2} < 2.0$ GeV, where $\mathcal{R} = \sqrt{(\Delta\eta)^2 + (\Delta\phi)^2}$ is the distance from the cluster center. The combined selection and isolation efficiency, ϵ_s , is estimated as a function of E_T^γ from a GEANT-based Monte Carlo simulation of the D0 detector. We find $\epsilon_s \sim 60\%$ (75%) in the CC (EC) at 8.0 GeV and $\epsilon_s \sim 88\%$ (90%) above 20 GeV. To minimize background from electrons, photon candidates are rejected if any tracks in the drift chamber extrapolate to within a road of width $\Delta\phi \times \Delta\theta = 0.2 \times 0.2$ defined by the angle subtended by the candidate photon cluster and the initial interaction vertex. The total charged tracking efficiency is estimated from $Z \rightarrow e^+e^-$ events to be 0.858 ± 0.013 (0.593 ± 0.079) in the central (forward) region.

The predominant background to direct photon production arises from the decay of π^0 or η mesons to two photons. The fraction of direct photons is determined from the energy (E_1) deposited in the innermost longitudinal section of the calorimeter, EM1. Photons have a small probability of showering in the material in front of the calorimeter and, thus, tend to deposit little energy in EM1. Sensitivity to the amount of EM1 energy can be used to distinguish multiple photon background from a single photon signal. We use the function $f(E_1) = \log_{10}[1 + \log_{10}\{1 + E_1(\text{GeV})\}]$ as our discriminant to determine the single photon purity. The expected distributions of this function for signal and background are found from events simulated with the PYTHIA Monte Carlo [9] and overlaid with data acquired using a random trigger to model noise, pileup, and multiple $p\bar{p}$ interactions. Three categories of fully simulated events are generated: those containing photons, and background events with and without charged tracks pointing from the interaction vertex to the EM cluster. The two different background samples are generated so that charged and neutral background fractions can be separately fit to the data, thus minimizing uncertainties from the tracking efficiency

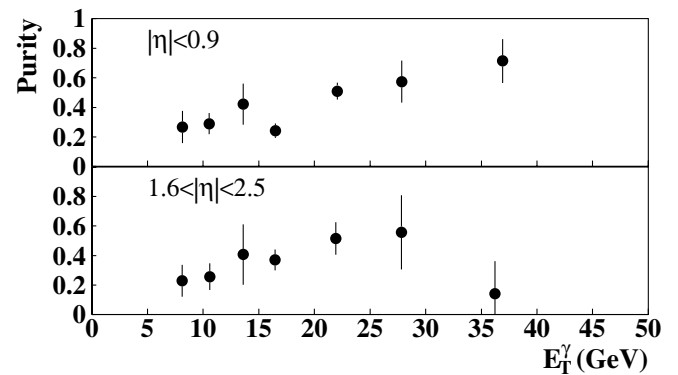


FIG. 2. The photon purity as a function of E_T^γ for central and forward photons. The error bars indicate the uncertainty in the fit purity and are larger than errors derived from statistical analysis alone.

and from the model used for jet fragmentation. A systematic uncertainty in modeling jet fragmentation is estimated by varying the multiplicity of neutral mesons in the core of PYTHIA jets by $\pm 10\%$. The detector response is modeled using a detailed GEANT simulation with the energy response in EM1 calibrated to match the data from $W \rightarrow e\nu$ events.

The same criteria used to select photon candidates in the data are applied to the Monte Carlo events. The distribution of f from the data is fitted to a normalized linear combination of Monte Carlo photons and background with and without charged tracks in the road pointing back to the interaction vertex. The fit is performed in different E_T^γ regions using the CERNLIB fitting package HMCMLL [10], with the fractions of signal and background constrained to be between 0.0 and 1.0. The purity is defined as the fraction of Monte Carlo photons in the normalized fitted distribution. A representative fit is shown in Fig. 1, and the photon purity as a function of E_T^γ is plotted in Fig. 2.

The final cross sections $d^2\sigma/dE_T^\gamma d\eta$, after applying efficiency and purity corrections, are shown in Fig. 3 and tabulated in Table I. The error bars show all uncorrelated uncertainties, which include the statistical uncertainty, and uncertainties from selection criteria, trigger efficiency, and

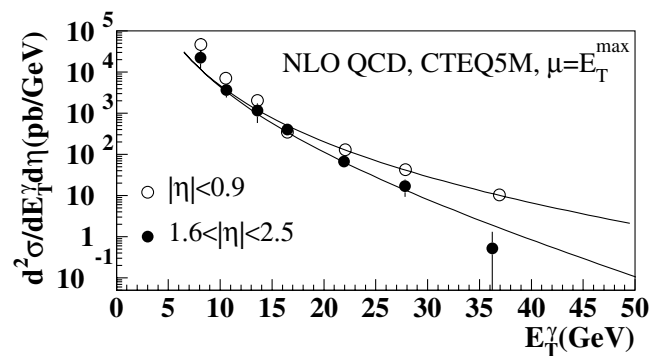


FIG. 3. The cross section for production of isolated photons in central and forward regions at $\sqrt{s} = 630$ GeV. The error bars show the total uncorrelated error, and the curves show cross sections predicted from NLO QCD.

TABLE I. The measured and predicted isolated photon production cross section at $\sqrt{s} = 630$ GeV. The value for the second column is determined according to Ref. [12]. The fifth and sixth columns are, respectively, the uncorrelated and correlated uncertainties.

E_T^γ Range (GeV)	Plotted E_T^γ (GeV)	$d^2\sigma/dE_T^\gamma d\eta$ (pb/GeV)		$\delta\sigma_U$ (%)	$\delta\sigma_C$ (%)
		Measured	NLO QCD		
$ \eta < 0.9$					
7.35–9.1	8.2	47 000	11 400	43	52
9.1–12.6	10.5	7160	3610	26	36
12.6–14.7	13.6	2040	1200	33	25
14.7–18.9	16.5	351	487	22	19
18.9–26.25	22.1	131	129	11	13
26.25–29.75	27.9	42.6	41.4	25	10
29.75–49.0	36.9	10.5	9.95	21	7
$1.6 < \eta < 2.5$					
7.35–9.1	8.1	22 400	11 200	48	42
9.1–12.6	10.6	3700	3310	35	31
12.6–14.7	13.6	1170	964	50	24
14.7–18.9	16.5	403	338	20	21
18.9–26.25	21.9	67.3	65.4	22	17
26.25–29.75	27.8	16.9	13.6	45	16
29.75–49.0	36.2	0.522	1.91	160	15

the fitted photon purity. The contribution from the fit to photon purity is the largest source of uncorrelated uncertainty. The correlated uncertainty consists of the uncertainties in luminosity, tracking efficiency, geometric acceptance, calorimeter energy scale, and the largest contribution, that from the fragmentation model.

The results are compared with NLO QCD calculations using CTEQ5M parton distributions [11], with renormalization and factorization scales $\mu_R = \mu_F = E_T^{\max}$, where E_T^{\max} is the maximum photon transverse energy in the event. Figure 4 compares the data and theory. A covariance matrix χ^2 provides a measure of the probability that the theory describes the data. A complete covariance

matrix, composed of correlated and uncorrelated uncertainties, is determined and the theoretical cross section is compared to the data with a χ^2 value of 11 (4.6) for 7 degrees of freedom in the CC (EC) region. This gives a standard χ^2 probability that the theory is consistent with the data at 12% (71%) probability in the CC (EC) regions. Deviations between theory and data are largest at low E_T^γ in the central region. These results are in qualitative agreement with those previously published at $\sqrt{s} = 1800$ GeV, where the theory is lower than the data at low E_T^γ (≈ 10 – 40 GeV) in the CC, but is consistent with the data over all E_T^γ in the EC [3]. Using different PDFs changed the cross section by less than 5% [13]. Setting scales to $\mu_R = \mu_F = 2.0E_T^{\max}$ or $\mu_R = \mu_F = 0.5E_T^{\max}$

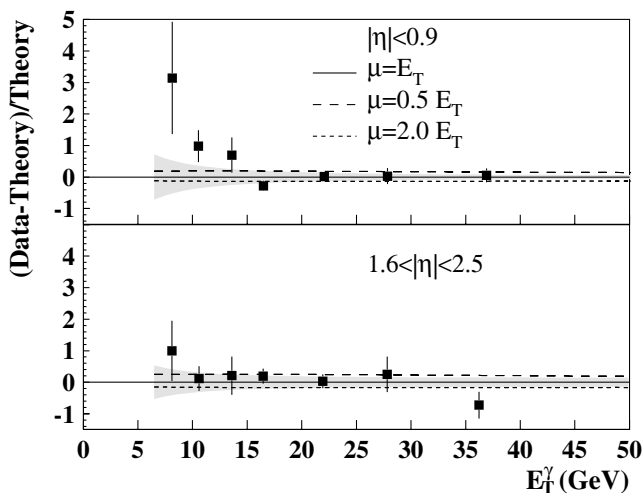


FIG. 4. Comparison of the measured cross section for production of isolated photons at $\sqrt{s} = 630$ GeV with NLO QCD using CTEQ5M parton distribution functions. The error bars indicate the uncorrelated uncertainty and the shaded bands indicate the correlated uncertainty.

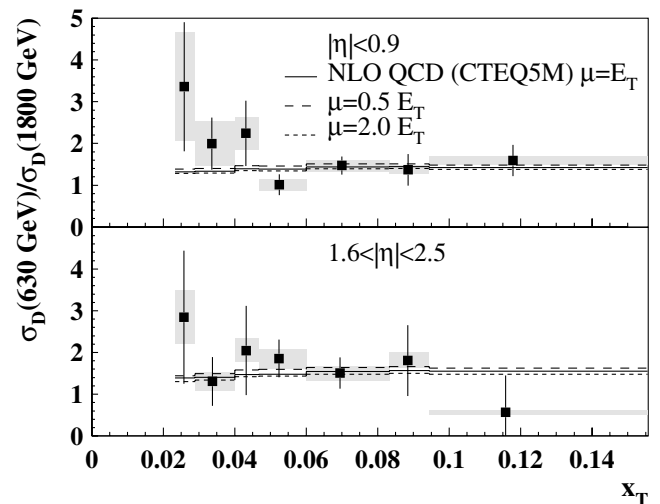


FIG. 5. The ratio of the dimensionless cross sections, $\sigma_D(\sqrt{s} = 630 \text{ GeV})/\sigma_D(\sqrt{s} = 1800 \text{ GeV})$. The error bars indicate the uncorrelated uncertainty and the shaded bands indicate the correlated uncertainty.

TABLE II. The measured ratio and NLO QCD prediction for the dimensionless cross section at $\sqrt{s} = 630$ GeV to that at $\sqrt{s} = 1800$ GeV. The columns labeled $\delta\sigma_U$ and $\delta\sigma_C$ are the uncorrelated and correlated uncertainties, respectively.

x_T Range	Plotted x_T	Ratio	Theory	$\delta\sigma_U$ (%)	$\delta\sigma_C$ (%)
$ \eta < 0.9$					
0.023–0.029	0.026	3.36	1.32	46	39
0.029–0.040	0.034	2.00	1.34	31	27
0.040–0.047	0.043	2.24	1.40	35	18
0.047–0.060	0.053	1.01	1.39	25	13
0.060–0.083	0.070	1.47	1.44	15	9
0.083–0.094	0.089	1.37	1.45	27	8
0.094–0.156	0.118	1.59	1.42	23	7
$1.6 < \eta < 2.5$					
0.023–0.029	0.026	2.84	1.39	56	22
0.029–0.040	0.034	1.31	1.41	45	17
0.040–0.047	0.043	2.05	1.47	52	14
0.047–0.060	0.052	1.86	1.48	24	13
0.060–0.083	0.070	1.51	1.54	24	11
0.083–0.094	0.088	1.81	1.57	47	11
0.094–0.156	0.116	0.563	1.55	160	10

changed the cross section by about 20%, as shown in Fig. 4.

In the simple parton model, the dimensionless cross section $E_T^4 E \frac{d^3\sigma}{dp^3}$, as a function of $x_T = \frac{2E_T}{\sqrt{s}}$, is independent of \sqrt{s} . Although deviations from such naive scalings are expected, the dimensionless framework provides a useful context for comparison with QCD. The experimental dimensionless cross section, averaged over azimuth, becomes $\sigma_D = \frac{E_T^3}{2\pi} d^2\sigma/dE_T d\eta$. The ratio $\sigma_D(\sqrt{s} = 630 \text{ GeV})/\sigma_D(\sqrt{s} = 1800 \text{ GeV})$ is determined by combining the cross section reported in this Letter with the D0 measurement at $\sqrt{s} = 1800$ GeV [3,14]. The ratio is shown as a function of x_T in Fig. 5, and Table II, together with the NLO QCD prediction.

Comparison of the theoretical cross section ratio to the data, using the complete covariance matrix, gives a χ^2 value of 6.5 (3.0) for 7 degrees of freedom in the CC (EC), which corresponds to a standard χ^2 probability of 49% (89%) in the CC (EC) region. Although the lowest x_T points are systematically higher than NLO QCD predictions in both the CC and EC regions, the deviations are not significant in light of our combined statistical and systematic uncertainties, and there exists good agreement between the measured ratio and theory.

We have measured the production cross section for isolated photons in $p\bar{p}$ collisions at $\sqrt{s} = 630$ GeV and compared this cross section with that measured at $\sqrt{s} = 1800$ GeV. The measurement is higher than the theoretical prediction at low E_T in the central rapidity region but agrees at all other E_T and in the forward rapidity region. The difference between data and theory is less significant for the ratio of cross sections, and the theory is consistent with the data over all E_T .

We thank W. Vogelsang and J.F. Owens for their assistance with the theoretical calculations. We thank the staffs

at Fermilab and collaborating institutions, and acknowledge support from the Department of Energy and National Science Foundation (U.S.A.), Commissariat à l'Énergie Atomique and CNRS/Institut National de Physique Nucléaire et de Physique des Particules (France), Ministry for Science and Technology and Ministry for Atomic Energy (Russia), CAPES and CNPq (Brazil), Departments of Atomic Energy and Science and Education (India), Colciencias (Colombia), CONACyT (Mexico), Ministry of Education and KOSEF (Korea), CONICET and UBACyT (Argentina), The Foundation for Fundamental Research on Matter (The Netherlands), PPARC (United Kingdom), Ministry of Education (Czech Republic), and the A.P. Sloan Foundation.

*Visitor from University of Zurich, Zurich, Switzerland.

- [1] J. Owens, Rev. Mod. Phys. **59**, 465 (1987).
- [2] UA2 Collaboration, J. Alitti *et al.*, Phys. Lett. B **263**, 544 (1991); UA2 Collaboration, R. Ansari *et al.*, Z. Phys. C **41**, 395 (1988).
- [3] D0 Collaboration, B. Abbott *et al.*, Phys. Rev. Lett. **84**, 2786 (2000).
- [4] CDF Collaboration, F. Abe *et al.*, Phys. Rev. Lett. **73**, 2662 (1994); CDF Collaboration, F. Abe *et al.*, Phys. Rev. D **48**, 2998 (1993).
- [5] J. Huston *et al.*, Phys. Rev. D **51**, 6139 (1995); H.-L. Lai and H.-N. Li, *ibid.* **58**, 114020 (1998); L. Apanasevich *et al.*, *ibid.* **59**, 074007 (1999).
- [6] M. Glück *et al.*, Phys. Rev. Lett. **73**, 388 (1994); W. Giele, in *Proceedings of the 5th International Symposium on Radiative Corrections, Carmel CA, 2000* (to be published electronically at <http://www.slac.stanford.edu/econf/>).
- [7] J. Krane, J. Bantley, and D. Owen, Report No. Fermilab-TM-2000, 1997 (unpublished).
- [8] D0 Collaboration, S. Abachi *et al.*, Nucl. Instrum. Methods Phys. Res., Sect. A **338**, 185 (1994).

- [9] T. Sjöstrand, *Comput. Phys. Commun.* **82**, 74 (1995).
- [10] R. Barlow and C. Beeston, *Comput. Phys. Commun.* **77**, 219 (1993).
- [11] H. Baer, J. Ohnemus, and J.F. Owens, *Phys. Rev. D* **42**, 61 (1990); W. Vogelsang and A. Vogt, *Nucl. Phys.* **B453**, 334 (1995). The authors of these predictions have verified that their calculated cross sections are consistent over the range of photon transverse energies measured here.
- [12] G.D. Lafferty and T.R. Wyatt, *Nucl. Instrum. Methods Phys. Res., Sect. A* **355**, 541 (1995).
- [13] CTEQ5M, CTEQ5HJ, MRST, MRSTg \uparrow , and MRSTg \downarrow were compared. For MRST, see A.D. Martin *et al.*, *Eur. Phys. J. C* **14**, 133 (2000).
- [14] The cross section at 1800 GeV is increased by 3.4% from the published result to account for the current value of the proton-antiproton total cross section as per D0 Collaboration, B. Abbott *et al.*, *Phys. Rev. D* **61**, 072001 (2000); E811 Collaboration, C. Avila *et al.*, *Phys. Lett. B* **445**, 419 (1999).